J Appl Electrochem (2008) 38:1089–1096
DOI 10.1007/s10800-008-9568-5

ORIGINAL PAPER

Amperometric/potentiometric hydrocarbon sensors: real world solutions for use in ultra high vacuum

Georgios Kyriakou · Amy V. Stevens · David J. Davis · Robert B. Grant · Mintcho S. Tikhov · Richard M. Lambert

Received: 1 November 2007 / Revised: 8 April 2008 / Accepted: 9 April 2008 / Published online: 29 April 2008

Abstract Carbonaceous deposits produced on Ru-capped multilayer mirrors under extreme ultra violet irradiation in the presence of adventitious gaseous hydrocarbons are a major obstacle to process implementation of EUV lithography. Here, by means of synchrotron radiation and laboratory measurements we show how carbon contamination occurs as a result of photoelectron-induced surface chemistry. We also demonstrate how a device based on an oxygen ion conducting solid electrolyte can act as a sensitive and reproducible sensor for detection of trace amounts of hydrocarbons in high vacuum environments.

Keywords Sensor · Oxygen XPS · Electrochemistry · Electrode · Platinum

1 Introduction

Surface contamination of critical components by adsorption of organic molecules can seriously compromise the integrity of costly high vacuum process technologies such as extreme ultraviolet (EUV) lithography which is the next step in the semiconductor device fabrication industry. This technology depends on the application of Ru-capped multilayer mirrors whose reflectivity rapidly degrades in the presence of hydrocarbons in the high vacuum environment. Similar contamination issues arise in high vacuum based electron lithographic processes. This report aims to revise our recent work regarding contamination issues arising in EUV lithography. Specifically we will present our work on (i) the elucidation of the processes that give rise to EUV-induced carbon contamination of Ru-capped mirrors [1] (ii) the development of mitigation strategies that will enhance mirror lifetime [2] (iii) the development of compact, low cost, sensitive and selective hydrocarbon sensors that could be distributed throughout large fabrication plants in order to protect key components by triggering appropriate counter-measures whenever an unforeseen incident leads to unacceptably high hydrocarbon partial pressures [3, 4].

G. Kyriakou · A. V. Stevens · D. J. Davis · M. S. Tikhov · 2R. M. Lambert (✉)
Chemistry Department, Cambridge University, Cambridge CB2 1EW, UK
e-mail: rml1@cam.ac.uk

R. B. Grant
Lithography Subsystems, BOC EDWARDS, Manor Royal, Crawley, West Sussex, UK

2 Experimental

Ru contamination measurements were performed in a UHV chamber [1, 2] operated at a base pressure of 5×10^{-10} mbar and equipped with a quadrupole mass spectrometer, an Al/Mg VSW X-ray source anode and a VSW HA100 concentric hemispherical analyzer with a multichannel detector. XPS measurements were performed using Mg Kα radiation with a photoelectron exit angle of 45°. The Ru(0001) single crystal (10 mm diameter; thickness 0.5 mm) could be resistively heated to 1,500 K, the temperature being monitored by means of a 95% W/5% Re—74% W/26% Re thermocouple. Cleaning of the crystal surface was achieved by cycles of Ar^+ sputtering (1 keV, 4 μA) followed by annealing at 1,000 K. Electron irradiation was by means of a simple normal incidence source consisting of a negatively biased filament and a Wehnelt cylinder, with the sample held at ground potential. Chemicals were delivered to the sample via a 6 mm diameter collimator tube and reported pressures are

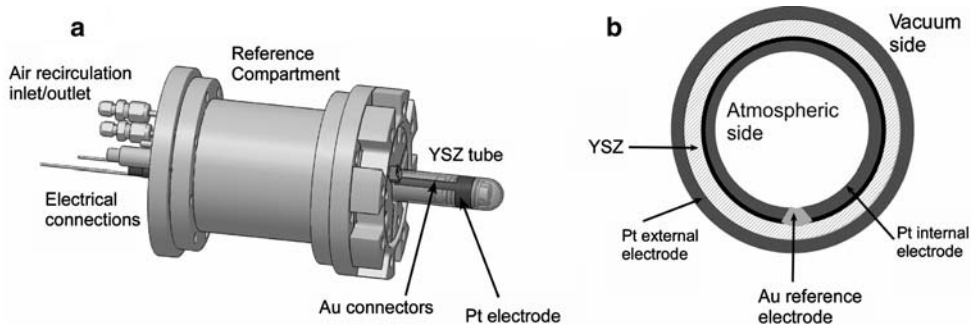

Fig. 1 (**a**) 3D schematic of the sensor body (Reproduced with permission from J. Phys. Chem. *B*, **2006**, *110*, 24571. Copyright 2006 American Chemical Society) (**b**) cross section of the sensing head

corrected for molecular ionization cross sections and collimator gain factor.

Sensor experiments were performed in a second UHV chamber using the device shown in Fig. 1 [3]. The experimental set-up provided a VG Quartz quadrupole mass spectrometer and X-ray photoelectron spectroscopy (XPS) capabilities with a dual Al/Mg anode and a single channel VSW HA100 concentric hemispherical analyser. The sensor consisted of an 8 mol% YSZ tube (FRIATEC) one end of which is closed; this is interfaced with an external Pt film that serves as the working (sensing) electrode, and an internal Pt film that serves as the counter electrode. A small Au reference electrode is located on the inner wall of the YSZ tube, all electrodes being deposited by DC sputtering. The outside of the YSZ tube is immersed in the UHV environment whose gas composition was to be analyzed whilst the inner (reference) compartment is maintained at atmospheric pressure by circulating air through it. The sensor assembly could be translated and rotated within the UHV chamber so as to optimise the position for XPS measurements. The YSZ tube was heated to operating temperature ($\sim$873 K) by an electrically insulated coil located against the inner wall of the YSZ tube. K-type thermocouples were used to monitor temperature at the surface of the working (sensing) electrode and within the reference compartment.

Chemicals *n*-pentane (99+%), *n*-hexane (99+%), *n*-heptane (99+%), *n*-octane (99+%) and toluene (99.8%) were obtained from Sigma-Aldrich and were further purified by freeze-pump-thaw cycles. 1-butene (99.9%) and *n*-butane (99+%) were obtained from BOC Special Gases; propane (99.95%) was obtained from Messer Gases.

3 Results and discussion

3.1 Ru contamination

We will first discuss the hydrocarbon triggered contamination of Ru surfaces [3]. The cause of adsorbate damage has been studied by Boller et al. [5] who showed that the contamination of a gold-capped EUV mirror under synchrotron radiation is due to the photoelectrons emitted from the mirror surface rather than the incident EUV radiation. We have therefore simulated the contamination of the Ru-capped multilayer mirror by examining the graphitic film growth on a Ru(0001) single crystal using various hydrocarbon molecules under low energy electron irradiation generated by an electron gun tuned at the appropriate energy [3].

Figure 2a shows the Ru 3d and the C 1 s emission spectra from the clean Ru(0001) and after exposure to toluene at a partial pressure of 3×10^{-7} mbar and under irradiation with 87.5 eV electrons ($\sim$2 mW mm^{-2}) for 150 min. It is apparent that the treatment results in attenuation of the Ru $3d_{5/2}$ (280.1 eV) and $3d_{3/2}$ (284.2 eV)

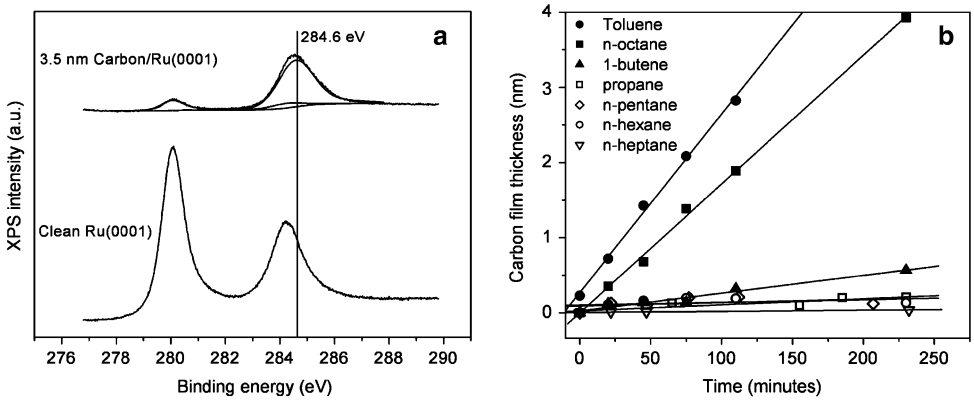

Fig. 2 (**a**) Ru 3d and C 1 s XP spectra of the clean Ru(0001) and after depositions with 3.5 nm Carbon (**b**) Electron-assisted uptakes of various hydrocarbons on Ru(0001) as monitored by XPS. (Reproduced with permission from J. Phys. Chem. *C*, **2007**, *111*, 4491. Copyright 2007 American Chemical Society)

intensities, whilst a new peak appears at a binding energy of 284.6 eV, characteristic of graphitic carbon [6]. Based on the attenuation of the Ru $3d_{5/2}$ signal ($I = I_o \exp(-d/\lambda\, cos\theta)$) the thickness of the carbon deposit is estimated as $\sim$3.5 nm assuming that a continuous graphitic multilayer of uniform thickness was formed. For this estimation we have used an inelastic mean free path value of 1.8 nm as determined specifically for graphite by Tanuma et al. [7]. Using the same procedure, the time dependence of *electron-assisted* carbon uptake by exposure to toluene, 1-butene, propane, *n*-pentane, *n*-hexane, *n*-heptane and *n*-octane at 343 K was measured (Fig. 2b). It is apparent that toluene and *n*-octane contaminate the surface at a significantly higher rate than the linear alkanes, up to and including *n*-heptane. Interestingly, the unsaturated species 1-butene contaminates the surface at a negligible rate, comparable to that observed for the shorter chain alkanes.

The results are understood in terms of the adsorption properties of the various hydrocarbons on the graphite-covered Ru surface. These are also believed to determine the rate at which the optical properties of Ru mirrors are degraded. We have shown that the graphite uptake rates can be accounted for satisfactorily in terms of the surface residence lifetimes of the various adsorbates on graphitic surfaces [1]. Linear alkanes of chain lengths up to C7 may be regarded as relatively benign, due to a low residence time whereas aromatics and alkanes > C8 would be highly detrimental.

Similarly we have recently demonstrated that in the presence of low energy electron irradiation corresponding to the photoelectron energy distribution encountered in practice, very low pressures ($\sim 10^{-5}$ mbar) of NO or O_2 are effective for oxidative removal of carbon from contaminated ruthenium surfaces at ambient temperature [2]. This procedure however may lead to the net accumulation of oxygen on and beneath the metal surface. In this case subsequent exposure of the resulting Ru surface to CO under electron irradiation leads to efficient removal of this oxygen, again at ambient temperature [2].

3.2 Sensing results

As discussed above, process control in systems like the EUV tool would be greatly enhanced by the availability of high vacuum compatible gas sensors [3, 4, 8]. Here we will show how an oxygen ion conducting solid electrolyte sensor can be used as a sensitive quantitative hydrocarbon sensor. Hydrocarbon sensing is a major research field [9] and the prototype sensor described in this article is based on the established technology of the lambda oxygen probe [10, 11]. We will first present the key characteristics of the device and then the detection procedure under potentiometric [3] and amperometric [4] operation modes.

3.2.1 *Oxygen control on the working electrode*

Allowing the sensor to equilibrate under open circuit conditions at 883 K in the absence of contaminants in the UHV compartment always resulted in a carbon-free, oxygen-containing working electrode as observed by XPS. This result is due to spontaneous oxygen semipermeation because YSZ, at high temperatures and under large oxygen partial pressure differences between the sampling and reference side, exhibits some electronic conductivity [12, 13]. In fact this property of the system provides a recovery mechanism for clean-off of the working electrode after operation in sensing mode. Since the rate of semi-permeation depends on the temperature and the oxygen partial pressure difference, an increase of hydrocarbon partial pressure on the UHV side is not expected to increase the semi-permeation rate. Instead a new steady state potential is achieved due to the removal of semi-permeated oxygen by the hydrocarbon. The corresponding clean surface values of $V^o_{WR}$and V^o_{WC} (open circuit steady state potential differences) were ~ -0.5 and -0.4 V, respectively. The working temperature of 883 K was chosen to ensure sufficient ionic conductivity in the YSZ.

The use of a galvanostat/potentiostat enables control of the oxygen concentration at the sensing (working) electrode as monitored by in situ XPS. Using the potentiostat, a potential $V_{WR} > V^o_{WR}$ can be imposed between the working and the reference electrode which results in oxygen being electro-pumped *towards* the working electrode. On the other hand setting $V_{WR} < V^o_{WR}$ results in electro-pumping of oxygen *away* from the working electrode. This approach is similar to that of the common current-limited sensors approach reported in the literature [14] in that a constant potential, V_{WR}, is applied and the resulting measured current, I_{WC}, can be related to the hydrocarbon partial pressure. *Our approach is novel because the working and counter electrodes are held in separate compartments* (under UHV and atmospheric pressure, respectively) and therefore it is not necessary to limit the diffusion of the electroactive oxygen to the counter electrode.

Alternatively, using the galvanostat, oxygen can also be electro-pumped towards or away the working electrode by applying a constant anodic current or cathodic current (I_{WC}), respectively between the working and counter electrodes. In all cases the current, I_{WC}, passed between the working and counter electrodes provides a quantitative measure of the rate of oxygen pumping.

Figure 3a shows O 1 s XP spectra obtained from the surface of the working electrode under potentiostatic operation [4]. It is immediately apparent that a stepwise decrease in V_{WR} results in a progressive reduction in the amount of oxygen present on the working electrode. The O 1 s spectrum consists of a broad feature that can be fitted

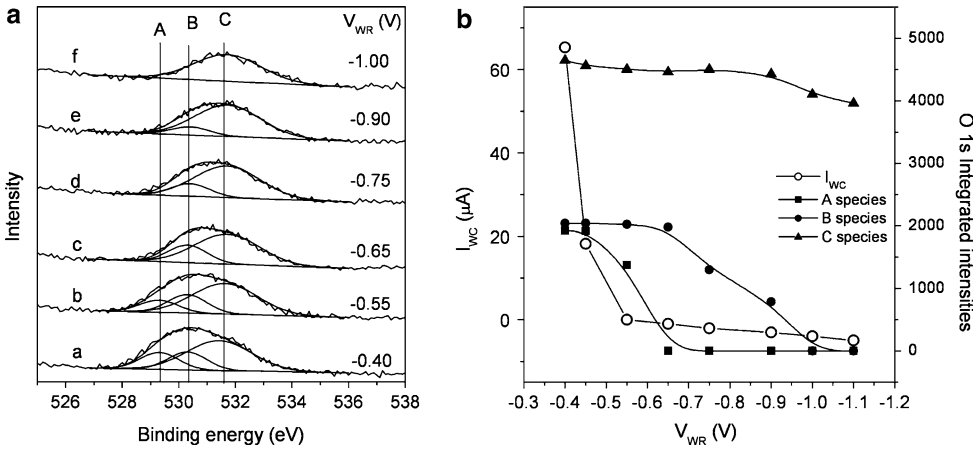

Fig. 3 (**a**) O 1 s XP spectra as a function of V_{WR} (**b**) I_{WC} and O 1 s integrated intensities as a function of V_{WR}. (Reproduced with permission from J. Phys. Chem. *C*, **2007**, *111*, 1491. Copyright 2007 American Chemical Society)

satisfactorily with the following three components [3, 4]: component B centered at 530.4 eV which corresponds to chemisorbed oxygen adatoms [15], C centered at 531.8 eV which corresponds to a Pt oxide species [16] (Pt oxide species have previously been detected at high temperatures on solid oxide supports by means of O_2 TPD [17]), species A centered at 529.4 eV reported by others has been assigned to spillover oxygen most likely of "ionic" nature on the Pt surface [18] (Oxygen in the underlying YSZ is XPS invisible due to the thickness of the Pt film and the near-normal photoelectron detection geometry).

Figure 3b shows the steady state integrated XPS intensities of the aforementioned species (A, B, C) at each value of V_{WR}, together with the measured corresponding steady state current, I_{WC}. The direction of oxygen anion flow through the solid electrolyte is reflected in the sign of this current: $I_{WC} > 0$ indicates O^{2-} moving towards the working electrode whilst $I_{WC} < 0$ denotes O^{2-} movement towards the counter electrode. The steady state oxygen coverage results from the balance between the rate of supply of electrochemically pumped oxygen and its rate of removal by either catalytic reduction by gaseous species (background CO + H_2, deliberately added hydrocarbons) or its desorption as O_2(g). Upon application of a given V_{WR} the system responds by altering the concentration of electro-active oxygen species present on the working electrode. We find that as V_{WR} is increased from −1.10 to −0.55 V the coverage of O_a (species B) increases approximately linearly and becomes saturated at $V_{WR} \sim -0.65$ V. The associated I_{WC} remains low but increases at a slow rate corresponding to the rate of oxygen pumping that is required to maintain a particular steady oxygen coverage in the presence of the oxidation reactions that act to deplete the oxygen coverage. Once O_a reaches its saturation coverage ($V_{WR} \sim 0.65$ V) a sharp increase in both the integrated intensity of the "ionic" oxygen (species A) and I_{WC} is found. This is accompanied by the increased production of gaseous oxygen in the UHV chamber. This behavior may be understood as follows [4]: electro-pumped oxygen ions spillover from the YSZ onto the Pt surface creating an "ionic" species (A) which rapidly transforms to O_a (species B). Within the range $-1.10\ \text{V} < V_{WR} < -0.65\ \text{V}$ the coverage of O_a builds up on the Pt and the amount of A remains small. Once the Pt surface is saturated with O_a, oxygen starts to accumulate at the three phase boundary and the amount of species A rises sharply. This interfacial oxygen undergoes recombination and desorption to yield O_2(g) necessitating a sharp increase of I_{WC} . Notice from Fig. 3b that the difference in overpotential between the clean and O_a saturated Pt surface is ~ -0.35 V. This is close to the change in work function ($\Delta\phi \sim 0.3$ eV [19]) induced by saturating Pt(111) with O_a by adsorption of oxygen from the gas phase, an observation that is in excellent agreement with the theoretical prediction made by Vayenas, namely $\Delta V_{WR} = \Delta\phi$ [20].

3.2.2 *Potentiometric sensing*

Figure 4 illustrates the open circuit response of the sensor to increasing partial pressures of toluene [3]. The sensor response was followed in-situ by XPS and the O 1 s and C 1 s integrated intensities are presented alongside the V_{WR} measurements. Even for very low partial pressures of the hydrocarbon ($\sim 3 \times 10^{-9}$ mbar) the sensor shows a pronounced response. After each successive increase in the hydrocarbon partial pressure the V_{WR} decreases and slowly tends to equilibrate to a specific value. The difference between the initial and final steady state potentials constitutes the sensor response. The sensor voltage recovers to more positive values only when the exposure to the hydrocarbon is terminated. It is the semipermeation of oxygen to the working electrode that provides this means of recovery. The simultaneously acquired XP C 1 s and O 1 s spectra provide important confirmation of the proposed

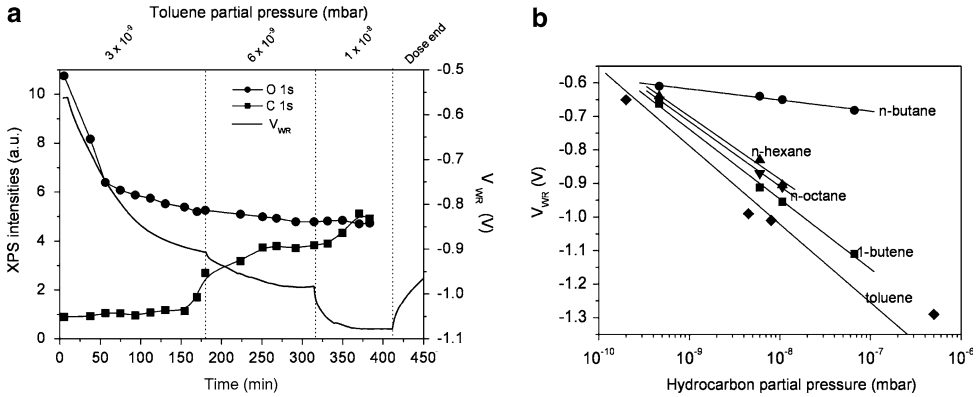

Fig. 4 (**a**) V_{WR} response to toluene as a function of pressure and time. Data are presented alongside the C 1 s and O 1 s integrated intensities (**b**) V_{WR} change as a function of hydrocarbon partial pressure for toluene, 1-butene, *n*-octane, *n*-hexane and *n*-butane. (Reproduced with permission from J. Phys. Chem. *B*, **2006**, *110*, 24571. Copyright 2006 American Chemical Society)

mode of sensing action. Successive increases of the hydrocarbon partial pressure result in further decreases (increases) in the O 1 s (C 1 s) intensities and thus altering the oxygen activity of the working electrode. Figure 4b shows the observed variation of V_{WR} with partial pressure for 1-butene, toluene, *n*-butane, *n*-hexane and *n*-octane. It is clearly evident that the sensor response varies linearly with the hydrocarbon partial pressure and that it is dependent on hydrocarbon functionality. The observed trends in rates of graphitic carbon accumulation are understandable in terms of the sticking coefficients for dissociative adsorption of the various hydrocarbon species [3, 5].

The relative advantages of each sensing mode are discussed in more detail in [3]. In summary, for the intended application a high sensitivity to low pressures of hydrocarbon is desirable. Open circuit operation produces greater responses than potentiometric operation with positive currents, I_{WC} but has the relative disadvantage that the response depends strongly on the initial background conditions.

3.2.3 *Amperometric sensing*

Finally the sensor can be operated in an amperometric mode [4]. In this operational mode a constant potential V_{WR} is applied between the working and the reference electrode that serves to maintain a set level of surface oxygen on the working electrode. In the presence of a hydrocarbon molecule, which acts to remove surface oxygen from the working electrode due to combustion, the potentiostat supplies a constant current in order to maintain the oxygen at the set level imposed by the applied V_{WR}. As the partial pressure of the target hydrocarbon molecule to be sensed increases the rate of the oxygen supply from the counter to the working electrode also increase and therefore the measured current I_{WC}. The effect is depicted in Fig. 5a where the differential response of the sensor to different hydrocarbons; the data were acquired at a $V_{WR} = -0.55$ V. It can be seen that toluene induces the strongest response, followed by *n*-octane; the alkanes induce responses that decrease with decreasing chain length. These relative responses are in good quantitative agreement with preliminary work studying the dissociative sticking probabilities of these same hydrocarbons on polycrystalline Pt [8].

The advantage of amperometric operation is that the measured current provides a direct measure of the hydrocarbon turnover rate on the sensing electrode, which is directly related to hydrocarbon partial pressure. With knowledge of the sticking coefficient of any given hydrocarbon on polycrystalline Pt at the relevant temperature (870 K) a simple treatment allows estimation of the hydrocarbon partial pressure by simply measuring I_{WC} [4]:

Assuming complete combustion of the hydrocarbon following the stoichiometric reaction:

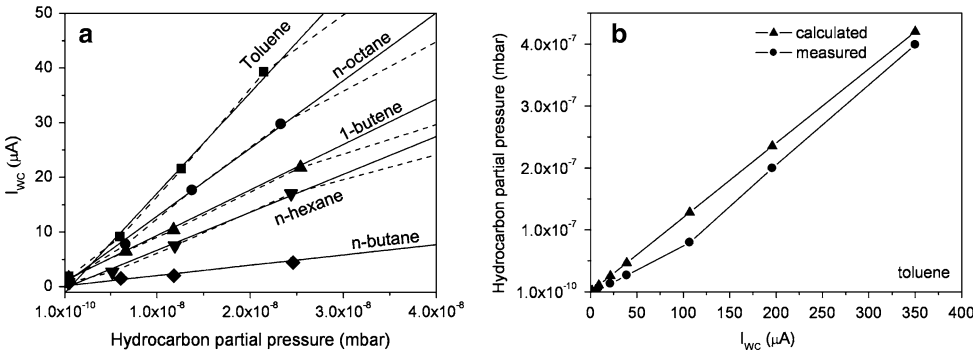

Fig. 5 (**a**) I_{WC} response to varying pressures of toluene, 1-butene, *n*-octane, *n*-hexane and *n*-butane (**b**) measured and calculated toluene partial pressures for given I_{WC} responses. (Reproduced with permission from J. Phys. Chem. *C*, **2007**, *111*, 1491. Copyright 2007 American Chemical Society)

$$C_xH_y + (2x + \frac{y}{2})O_{(a)}(Pt) \rightarrow xCO_2 + \frac{y}{2}H_2O \quad (1)$$

(Our assumption that O(a) (and not O^{2-}) is the oxidizing species is consistent with the plausible view that the hydrocarbon and the oxygen species should both be adsorbed on the same phase; moreover, this is strongly supported by the XPS data.) Then from kinetic theory, the flux of hydrocarbon molecules incident on the working electrode can be expressed by Eq. 2 while the delivery rate of oxygen anions to the working electrode can be calculated from the measured I_{WC} using Eq. 3

$$z = \frac{p}{(2\pi kTm)^{1/2}}A \quad (2)$$

$$N_{O^{2-}} = \frac{I_{WC}}{2F}N_A \quad (3)$$

where p is the hydrocarbon partial pressure, A is the area of the working electrode, k is Boltzmann's constant, m is the mass of the hydrocarbon and T is the temperature, $N_{O^{2-}}$ is the number of oxygen anions electrochemically pumped to the working electrode, F is the Faraday constant and N_A is Avogadro's number. Taking into account the sticking coefficient of the hydrocarbon, S_H, then the combination of Eqs. 2 and 3 provides the following expression relating the hydrocarbon partial pressure to the measured I_{WC}:

$$I_{WC} = \frac{2p(2x + \frac{y}{2})}{N_A\sqrt{2\pi kTm}}AFS_H \quad (4)$$

Figure 5b shows how measured and calculated toluene partial pressures vary as a function of I_{WC}: the agreement is very satisfactory. It should be noted that in our laboratories we have recently studied the effect of the presence of combustion products CO, CO_2 and H_2O on the sensor response to hydrocarbons and initial experiments have shown that there is negligible change. Further measurements are in progress and will be reported in future publications.

3.3 Bimetallic surfaces for selectivity enhancement

Pt electrodes provide only a small degree of selectivity between "harmful" and "benign" hydrocarbons. Therefore, for application purposes, it would be beneficial if the device could be fitted with electrode systems capable of better discrimination between different hydrocarbon moieties. We have tried to simulate such electrode systems by studying the dissociative adsorption of hydrocarbons on bimetallic Pt-Au systems [21]. Au was chosen as an initial alloying metal due to its inert behaviour towards hydrocarbon decomposition and therefore strongly contrasting behavior to Pt. A summary of our key observations are given below.

A range of Au/Pt surfaces were prepared by first depositing ~2.2 ML of Au onto a Pt polycrystalline sample at room temperature and then annealing to successively higher temperatures (between 1,000 K and 1,155 K) for 5 min at each temperature. This procedure caused progressive in-diffusion of Au into the Pt, monitored by the decrease (increase) of the Au 4f (Pt 4f) signal. Following this method different Au/Pt surface alloys of specific composition were formed in a very reproducible manner. All alloy surfaces were stable at 870 K at which temperature all hydrocarbon uptakes were performed. The hydrocarbons tested were toluene, 1-butene and *n*-hexane.

All three hydrocarbons gave immeasurably low carbon uptake at 870 K on a surface prepared by deposition of ~2.2 ML Au on the Pt substrate. With increasing thermal pre-treatment (i.e. increasing in-diffusion of Au) hydrocarbon adsorption and decomposition was triggered, in the order 1-butene, then toluene, then *n*-hexane. Figure 6 shows the dependence of carbon uptake on two Pt/Au alloys and pure Pt. The two alloy surfaces were made by annealing the initial Au deposit (~2.2 ML) to (a) 1,070 K (Alloy 1; Au 4f:Pt 4f = 0.21:1) and (b) 1,105 K Alloy 2; Au 4f:Pt 4f = 0.15:1). By making the crude approximation that all XPS-visible Au is located in the surface layer, then, taking account of photoionization cross sections [22], the surface gold contents of Alloys 1 and 2 are calculated as 0.80 and 0.75 ML, respectively. It is immediately apparent that the surface alloy behaves very differently from pure Pt. XPS characterization of the Pt/Au system coupled with CO adsorption/desorption experiments as a function of surface composition shows that the hydrocarbon sticking and decomposition occurs principally on surface sites consisting of Pt-rich ensembles of metal atoms [21] More importantly different uptake rates of the three hydrocarbons can be achieved depending on the distribution of Pt/Au surface ensembles. In principle electronic effects could also play a role, however both theory [23] and experiment [24] indicate that in the bimetallic system Pt is only weakly perturbed by Au.

Extending our work on Pt/Au alloys, a sensor body has been built similar to that shown in Fig. 1 but with a Pt/Au working electrode. The sensing performance of this arrangement is currently being tested and will be reported in future publications. It is expected that future extension to alternative alloying metals will have similar encouraging consequences for the discrimination of hydrocarbons. The eventual aim of our project is the development of sensor array devices in which the elements have overlapping but different selectivity profiles.

4 Conclusions

1. We have successfully simulated the photon induced chemistry of ambient contaminants on Ru capped MLM using low energy electrons and a Ru(0001) crystal. The contamination is determined by the

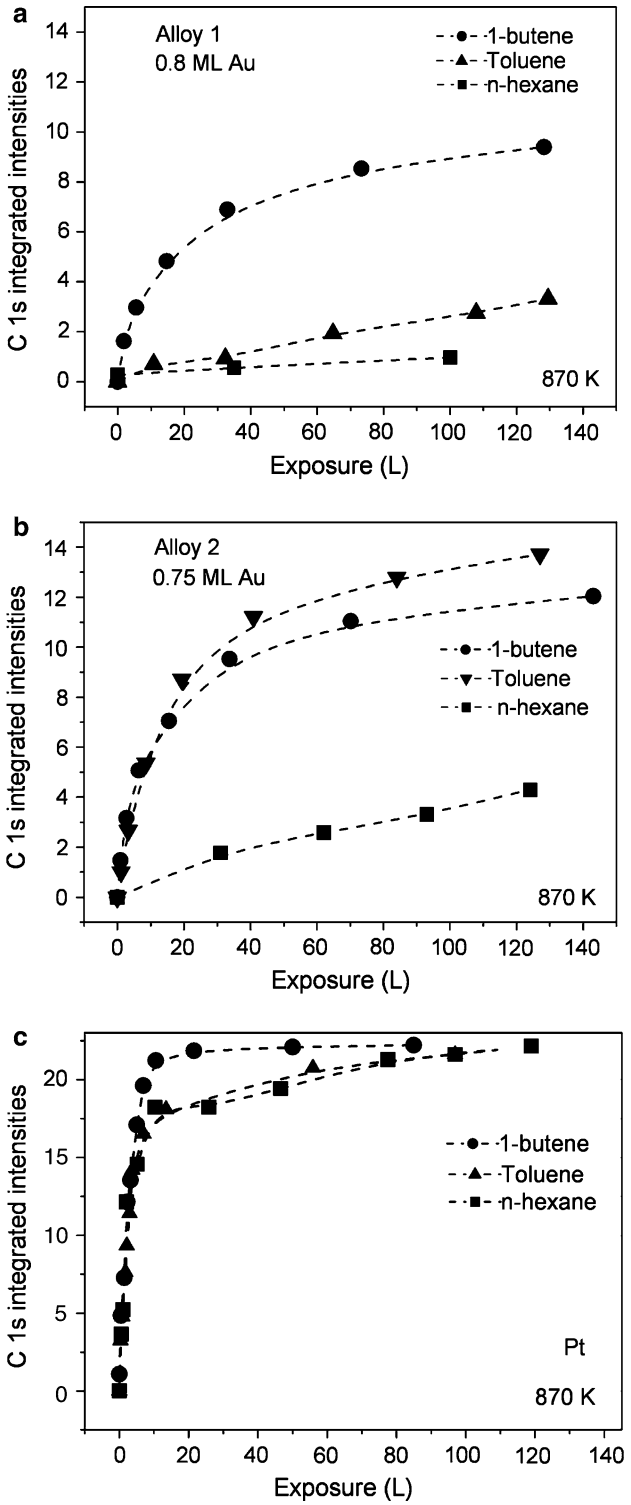

Fig. 6 Uptake of toluene, 1-butene and *n*-hexane on (**a**) Alloy 1 (0.8 ML Au) and (**b**) Alloy 2 (0.75 ML Au) and (**c**) clean Pt. Both alloy surfaces were prepared by deposition of 2.2 ML of Au at RT and subsequent annealing to 1,070 and 1,105 K respectively. (Reproduced with permission from J. Phys. Chem. *C*, **2006**, *110*, 11958. Copyright 2006 American Chemical Society)

surface residence time of the various molecules on a graphitic like surface.

2. We have constructed and successfully operated the first sensitive potentiometric/amperometric hydrocarbon sensor for high vacuum applications.
3. Polycrystalline, gold-rich, Au/Pt bimetallic surfaces are very promising for use as sensitive and *selective* hydrocarbon sensing electrodes for use in high vacuum environments. By choice of surface composition, they may be used to discriminate, variously, between alkanes, alkenes and aromatics.
4. We have developed novel methods for the in situ/ex situ remediation of Ru-capped multilayer mirrors: in the presence of low energy electron irradiation, NO and O_2 are effective for oxidative removal of carbon from contaminated Ru surfaces while CO is effective for oxide removal. The procedure takes place at ambient temperature.

Acknowledgements The authors acknowledge funding from BOC Edwards and the UK Engineering and Physical Sciences Research Council (EPSRC).

References

1. Kyriakou G, Davis DJ, Grant RB, Watson DJ, Keen A, Tikhov MS, Lambert RM (2007) J Phys Chem C 111:4491
2. Davis DJ, Kyriakou G, Grant RB, Tikhov MS, Lambert RM (2007) J Phys Chem C 111:12165
3. Kyriakou G, Davis DJ, Grant RB, Tikhov MS, Keen A, Pakianathan P, Lambert RM (2006) J Phys Chem B 110:24571
4. Davis DJ, Kyriakou G, Grant RB, Tikhov MS, Lambert RM (2007) J Phys Chem C 111:1491
5. Boller K, Haelbich RP, Hogrefe H, Jark W, Kunz C (1983) Nucl Instrum Method 208:273
6. Moulder JF, Stickle WF, Sobol PE, Bomben KD, (1995) Handbook of X-ray photoelectron spectroscopy physical electronics. Perkin-Elmer, Minnesota
7. Tanuma S, Powell CJ, Penn DR (2004) Surf Interface Anal 36:1
8. Kyriakou G, Davis DJ, Lambert RM (2006) Sens Actuators B Chem 114:1013
9. Lawrence N (2006) Talanta 69:385
10. Fleming WJ (1977) J Electrochem Soc 124:21
11. Radhakrishann R, Virkar AV, Singhal SC, Dunham GC, Marina OA (2005) Sens Acuators B 105:312
12. Sridhar KR, Blanchard JA, (1999) Sens Actuators B 59:60
13. Fujiwara Y, Kaimai A, Hong J, Yashiro K, Nigara Y, Kawada T, Mizusaki J (2003) J Electrochem Soc 150:E117
14. Eguchi Y, Watanabe S, Kubota N, Takeuchi T, Oshihara T, Takita Y (2000) Sens Actuators B 66:9
15. Luerßen B, Günther S, Marbach H, Kiskinova M, Janek J, Imbihl R (2000) Chem Phys Lett 316:331
16. Aita CR, Tran Ngoc C (1984) J Appl Phys 56:958
17. Yoshida H, Nonoyama Y, Yazawa Y, Hattori T (2005) Physica Scripta T115:813
18. Vayenas CG, Lambert RM, Ladas S, Bebelis S, Neophytides S, Tikhov MS, Filking NC, Makri M, Tsilpakides D, Cavalca C, Besocke K (1997) Studies Surf Sci Catal 112:39

19. Derry GN, Ross PN, (1986) J Chem Phys 82:2772
20. Vayenas CG, Bebelis S, Ladas S, (1990) Nature 343:625
21. Davis DJ, Kyriakou G, Lambert RM (2006) J Phys Chem B 110:11958
22. Yeh JJ, Lindau I, (1985) Atomic Nucl Data Tables 32:1
23. Persden MØ, Helveg S, Ruban A, Stensgaard I, Lægsgaad E, Nørskov JK, Besenbacher F (1999) Surf Sci 426:395
24. Sachtler JWA, Somorjai GA (1983) J Catal 81:77